Molecular dynamics simulation of the electrokinetic flow of an aqueous electrolyte solution in nanochannels

Hiroaki Yoshida,[1,2,a)] Hideyuki Mizuno,[3] Tomoyuki Kinjo,[1,2] Hitoshi Washizu,[1,2] and Jean-Louis Barrat[3,4]

[1)] *Toyota Central R&D Labs., Inc., Nagakute, Aichi 480-1192, Japan*

[2)] *Elements Strategy Initiative for Catalysts and Batteries (ESICB), Kyoto University, Katsura, Kyoto 615-8520, Japan*

[3)] *Laboratory for Interdisciplinary Physics, UMR 5588, Université Grenoble 1 and CNRS, 38402 Saint Martin d'Hères, France*

[4)] *Institut Laue–Langevin, 6 rue Jules Horowitz, BP 156, 38042 Grenoble, France*

(Dated: 1 March 2022)

Electrokinetic flows of an aqueous NaCl solution in nanochannels with negatively charged surfaces are studied using molecular dynamics (MD) simulations. The four transport coefficients that characterize the response to weak electric and pressure fields, namely the coefficients for the electrical current in response to the electric field (M^{jj}) and the pressure field (M^{jm}), and those for the mass flow in response to the same fields (M^{mj} and M^{mm}), are obtained in the linear regime using a Green–Kubo approach. Nonequilibrium simulations with explicit external fields are also carried out, and the current and mass flows are directly obtained. The two methods exhibit good agreement even for large external field strengths, and Onsager's reciprocal relation ($M^{\mathrm{jm}} = M^{\mathrm{mj}}$) is numerically confirmed in both approaches. The influence of the surface charge density on the flow is also considered. The values of the transport coefficients are found to be smaller for larger surface charge density, because the counter-ions strongly bound near the channel surface interfere with the charge and mass flows. A reversal of the streaming current and of the reciprocal electro-osmotic flow, with a change of sign of M^{mj} due to the excess co-ions, takes places for very high surface charge density.

[a)]Electronic mail: h-yoshida@mosk.tytlabs.co.jp

I. INTRODUCTION

Power generation and energy storage technology that utilize electrochemical devices, such as the lithium-ion battery and the fuel cells, have been studied extensively, and their performance has continued to improve regularly. At the core of these electrochemical devices, one generally finds systems consisting of complex electrolyte solutions and of charged solids, e.g., the porous electrode layer in the lithium-ion battery[1] and the electrolyte membrane in the fuel cell.[2] The transport of the ions and the solvent through the charged solid structure affects the total performance of the devices significantly, and thus the control and optimization of the transport phenomena are central areas of research in the development of innovative electrochemical devices.[3–5]

Transport phenomena are observed as flows of the ions and solvent in response to external driving forces. The driving forces important in electrochemical systems are those induced by the electric field and/or the pressure gradient.[6] If the system is close to the thermal equilibrium state so that the system responds linearly to the external fields, the electric current J and mass flow Q induced by the electric field and the pressure gradient are written in the following form:[7]

$$\begin{pmatrix} J \\ Q \end{pmatrix} = \begin{pmatrix} M^{\mathrm{jj}} & M^{\mathrm{jm}} \\ M^{\mathrm{mj}} & M^{\mathrm{mm}} \end{pmatrix} \begin{pmatrix} E_x \\ P_x \end{pmatrix}, \tag{1}$$

where E_x is the electric field and P_x is the mass acceleration representing the pressure gradient.[8] The coefficient M^{jj} corresponds to the effective electric conductivity, and M^{mm} is directly related to the permeability of the porous media.[9] On the other hand, M^{jm} and M^{mj} are the transport coefficients for the streaming current and the electro-osmotic flow. Onsager's reciprocal relation states that the values of these coefficients are identical, i.e., $M^{\mathrm{jm}} = M^{\mathrm{mj}}$ (see e.g., Refs 7, 10–13). The values of the transport coefficients are dependent on complex, multi-physics phenomena, namely the internal and external electric field, the solvent flow, and the diffusion and migration of ions. Furthermore, commonly used electrochemical systems exhibit a broad hierarchy of scales: whereas the atomic scale is important at the interface between the solid and the electrolyte solution, the thickness of the electrical double layer formed near the interface can extend to a few tens of nanometers, and the characteristic size in the porous media or membranes through which the electrolyte solution flows ranges from a few nanometers to tens of micrometers. It is therefore very difficult

to evaluate the values of the transport coefficients using a precise model that describes all of the physics included in the system. One strategy to overcome this difficulty is to incorporate the effect of the interface as boundary conditions for the macroscopic description with coarse-graining the events near the interface, and to evaluate the transport coefficients using equations based on the continuum theory.[7,14–16] Obviously, however, the macroscopic description is not always valid. When the relevant length scales decrease, the relative effect in the atomic scale becomes significant, and the theoretical predictions fail to reproduce the experimental observation.[17,18] In this case, since the characteristic scale approaches the atomic scale and the scale gap is less important, the molecular dynamics (MD) method, which deals explicitly with atoms, becomes accurate and efficient.[19] Applying realistic interaction forces between particles constituting ions, solvent molecules, and charged solids allows one to evaluate the transport coefficients by capturing accurately the phenomena taking place at interfaces.

Two methods are available to obtain the responses (current J and the mass flow Q) to external fields using MD simulations. One is to assume linear response, and to apply the Green–Kubo formulas.[12,20–22] The four transport coefficients are then obtained simultaneously using the results of MD simulations performed at thermal equilibrium, without any external force. Although the Green–Kubo formulas are only valid within the limit of the linear response regime, the real systems under usual conditions are most often operating within this limit, in view of the fact that the current and mass flow observed experimentally respond linearly to the external fields (e.g., Refs. 23 and 24). (For systems in which a nonlinear response is important, the transient time correlation function formalism is a possible alternative to the Green–Kubo approach.[25,26]) The other method is to directly observe the current and mass flow, after applying an explicit external field in the MD simulation.[27–31] This method is referred to as the direct method in the present paper. Since the direct method does not assume the system to be close to thermal equilibrium, the charge and mass flow can be obtained in response to external fields of arbitrary strength. Further, since the actual flows are induced in the simulations, detailed discussion on the profiles of flows is possible. However, the field strength attainable in laboratories is too small to distinguish the induced flows from the thermal fluctuation, and extremely strong external fields are necessary. Therefore, comparison with the results based on the linear response theory is inevitable, before extrapolating the results of the direct method to real systems.

In the present study, we apply the two methods to specific systems with realistic ions and solvent. More precisely, the behavior of an aqueous NaCl solution in a channel between two charged walls is investigated using MD simulations. The material of the wall is not specified, and simply corresponds to a generic hydrophilic material. Although the results of each method for similar systems have been reported,[21,27,28,31] a systematic comparison of the transport coefficients obtained using the Green–Kubo formulas with the results of the direct method is, to our knowledge, new. Here, we establish the protocol to evaluate the transport coefficients using the data from MD simulations, and we compare systematically the current and mass flow obtained through Eq. (1) using the transport coefficients with those obtained by using the direct method. In addition, the influence of the surface, which is important for the flow at a small scale, is investigated. Special attention is devoted to the effect of the surface charge density, because the counter-ion condensation at the charged surface must have important effects on the response.[32,33] The dependence of the effective electrical conductivity and of the flow rate in a Poiseuille geometry is examined, and the inversion of the streaming current and the electro-osmotic flow[27] is discussed.

II. MODELS AND METHODS

We consider an aqueous NaCl solution between two charged walls, as shown in Fig. 1. Each wall consists of two-dimensional equilateral triangular lattice of a model atom, say atom A, with shortest distance between two atoms being ℓ. In the present study, ℓ is fixed at 3 Å. Among the wall atoms, every ℓ_c/ℓ atoms in the direction of the shortest distance are negatively charged with one elementary charge $(-e)$. The absolute value of the surface charge density is then expressed as $\sigma = 2e/\ell_c^2\sqrt{3}$. Since in the present study the walls are always negatively charged, the surface charge density given in the following refers to its absolute magnitude. The electrolyte solution contains N^{Cl} Cl^- ions and N^{Na} Na^+ ions. The relation $N^{\mathrm{Na}} = N^{\mathrm{Cl}} + N^{\mathrm{Ac}}$ holds with N^{Ac} being the number of charged atom A, because of the electrical neutrality.

The extended simple point charge (SPC/E) model[34] is employed to describe the interactions between water molecules. The interactions between ions are described simply by a sum of electrostatic and Lennard-Jones (LJ) potentials, with parameters taken from Ref. 35. The LJ parameters for water-ion and Na-Cl pairs are determined by the Lorentz–Berthelot

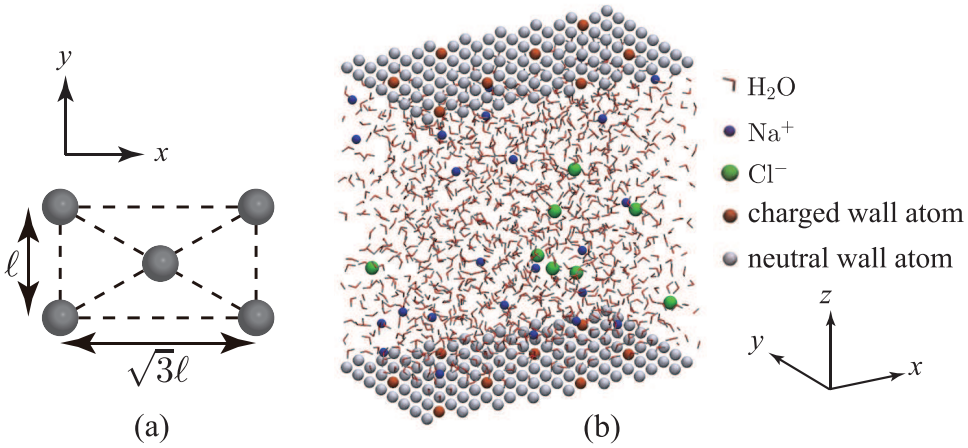

FIG. 1. (a) A unit cell of the equilateral triangular lattice of the wall atoms in the x-y plane. (b) A snapshot of the system at equilibrium.

TABLE I. Parameters for interaction between atom A and a water molecule.

interaction	m	n	r_0 [Å]	ϵ [kcal/mol]	η
A–O	6	12	3.85	0.25	2.34
A–H	8	12	2.14	1.52	2.34

mixing rule.[12,36] For the interaction between a wall atom A and a water molecule, we employ the following potential φ:[37]

$$\varphi(r) = \frac{\eta\epsilon}{n-m}\left(m\left(\frac{r_0}{r}\right)^n - n\left(\frac{r_0}{r}\right)^m\right), \tag{2}$$

where r is the distance between atoms, and r_0 is the distance at which φ/η takes the minimum value $-\epsilon$; m and n are integers. The values of the parameters used in the simulation are listed in Table I. The factor $\eta = 2.34$ common to A-Hydrogen and A-Oxygen interactions was determined such that the binding energy between an SPC/E molecule and the triangular lattice of atom A was equal to that of the lowest energy between two SPC/E molecules (-7.5 kcal/mol). Then, the model surface employed here represents a hydrophilic surface within the limitation of homogeneously distributed sites. Note that in real systems the hydrophilic sites are distributed more heterogeneously.[38] In calculating the LJ interaction forces between a wall atom A and an ion, the mixing rule mentioned above is employed, with the LJ parameters of the neutral and charged wall atoms being the same as those of the SPC/E model and the Cl^- ion, respectively.

The MD simulations are carried out using the open-source code LAMMPS.[39,40] During the simulations, the number of particles and the volume V are kept constant while the temperature $T = 300\,\mathrm{K}$ is maintained using the Nosé–Hoover thermostat (NVT ensemble). The time step is 1 fs throughout this paper, with using SHAKE algorithm[41] to maintain the SPC/E water molecules rigid. The LJ interactions are treated using the standard method of spherical cutoff (cutoff radius = 9.8 Å), while long-range Coulomb interactions are treated by using the particle-particle particle-mesh (PPPM) method. In order to treat the slab geometry, the method proposed by Yeh and Berkowitz[42] is employed, i.e., the z direction is first extended to create empty spaces outside the channel, then the periodic boundary conditions are applied; the artifacts from the image charges due to periodic boundary conditions in the z direction are removed by adding a correction force to each particle.

The distance H between the upper and lower walls is determined such that the normal pressure is equal to the atmospheric pressure, in the following manner: first the water molecules and the ions are randomly distributed at a density lower than that at atmospheric pressure, and an MD simulation is carried out with this configuration as an initial condition. During the simulation, the atoms of the upper wall are constrained such that they move only in the z direction, while the atoms of the lower wall are completely frozen. At each time step, the forces in the z direction felt by all of the upper-wall atoms are averaged (denoted by $\bar{f}_{wz}$). Then the forces acting on the upper-wall atoms are replaced by the common force $\bar{f}_{wz} - f_0$, with f_0 being the force per atom corresponding to the atmospheric pressure. Typically it takes 10 ps for $\bar{f}_{wz} - f_0$ to reach zero, after which it fluctuates. The simulation is continued for 0.6 ns, and the average value of the distance between the upper and lower walls, over the interval $0.1 < t < 0.6\,\mathrm{ns}$, is chosen as H. The configuration obtained after 1 ns equilibration time, with the upper- and lower-wall atoms being frozen at a distance H, is used as the initial condition for the following simulations.

In the present study, MD simulations under explicit external fields (direct method), as well as equilibrium simulations, are carried out. The forces acting on ith particle due to the external fields are given by

$$F_{xi}^{E} = q_i E_x, \tag{3}$$

$$F_{xi}^{P} = m_i P_x, \tag{4}$$

where q_i and m_i are respectively the charge and the mass of ith particle, E_x is the electric field in the x direction, and P_x is the mass acceleration for simulating the force due to the pressure gradient while applying periodic boundary conditions. The relation between P_x and the pressure field p is $P_x = -(1/\rho_0)(\mathrm{d}p/\mathrm{d}x)$ (ρ_0: the average density). The responses to the fields, namely the charge flux j_x and the mass flux c_x, are obtained from the MD trajectory as

$$c_x = \sum_i m_i \dot{x}_i, \tag{5}$$

$$j_x = \sum_i q_i \dot{x}_i, \tag{6}$$

where the summation runs over all particles.

III. THE GREEN–KUBO FORMULAS

The current density $J = j_x/V$ and the mass flow density $Q = c_x/V$ under the fields E_x and P_x are obtained using Eq. (1) for the system within the limit of the linear response regime, as described in Introduction. The transport coefficients M^{ij}, M^{jm}, M^{mj}, and M^{mm} are related to the time-correlation functions of the charge and mass fluxes via the Green–Kubo formulas based on the linear response theory.

In order to derive the specific forms of the Green–Kubo formulas for the system considered in the present study, we follow the standard discussion of the linear response theory.[12] The Hamiltonian of the system $\mathcal{H}$ under a weak external field $\mathcal{F}_0$ is perturbed by $\mathcal{H}'(t)$ from the value at the thermal equilibrium state $\mathcal{H}_{\mathrm{eq}}$:

$$\mathcal{H} = \mathcal{H}_{\mathrm{eq}} + \mathcal{H}'(t), \tag{7}$$

$$\mathcal{H}'(t) = -\mathcal{A}(\boldsymbol{r}^N)\mathcal{F}_0 \exp\left(-i\omega t\right), \tag{8}$$

where ω is the frequency of the external field, and $\mathcal{A}$ is a function of the particle positions

$\boldsymbol{r}^N$. Then, the change in the observed variable $\mathcal{B}$, denoted by $\Delta\mathcal{B}$, is expressed as

$$\langle \Delta\mathcal{B} \rangle = M^{BA}(\omega)\mathcal{F}_0 \exp(-i\omega t), \tag{9}$$

$$M^{BA}(\omega) = \frac{1}{k_{\mathrm{B}}T}\int_0^\infty \langle \mathcal{B}(t)\dot{\mathcal{A}} \rangle \exp(i\omega t)\mathrm{d}t, \tag{10}$$

where k_{B} is the Boltzmann constant. In the system considered herein, $\mathcal{F}_0 = E_x$ and $\mathcal{A} = \sum_i q_i x_i$ in the case of electric field, and $\mathcal{F}_0 = P_x$ and $\mathcal{A} = \sum_i m_i x_i$ in the case of mass acceleration. The observed variables are the current density $\mathcal{B} = J = j_x/V$, and the mass flow density $\mathcal{B} = Q = c_x/V$. Since a time-independent external field is considered ($\omega \to 0$), the transport coefficients are expressed in terms of j_x and c_x as follows:

$$M^{\mathrm{jj}} = \frac{1}{k_{\mathrm{B}}TV}\int_0^\infty \langle j_x(t)j_x(0) \rangle \mathrm{d}t, \tag{11}$$

$$M^{\mathrm{jm}} = \frac{1}{k_{\mathrm{B}}TV}\int_0^\infty \langle j_x(t)c_x(0) \rangle \mathrm{d}t, \tag{12}$$

$$M^{\mathrm{mj}} = \frac{1}{k_{\mathrm{B}}TV}\int_0^\infty \langle c_x(t)j_x(0) \rangle \mathrm{d}t, \tag{13}$$

$$M^{\mathrm{mm}} = \frac{1}{k_{\mathrm{B}}TV}\int_0^\infty \langle c_x(t)c_x(0) \rangle \mathrm{d}t. \tag{14}$$

Here, definition of M^{jj} is identical to that of the electrical conductivity, and M^{mm} is related to the permeability of the porous media : $k = \nu M^{\mathrm{mm}}/\rho_0$ (k: permeability, ν: kinetic viscosity).[9] The coefficients M^{jm} and M^{mj} are the measures of the streaming current and the electro-osmotic flow, respectively. Since the MD simulation is time reversible apart from the numerical error, Eqs. (12) and (13) are identical in the thermal equilibrium state, i.e., $M^{\mathrm{jm}} = M^{\mathrm{mj}}$, which is known as Onsager's reciprocal relation.[7,10–13]

IV. RESULTS AND DISCUSSION

A. Evaluation of the transport coefficients

We first apply the Green–Kubo formulas (11) through (14) to a specific system with an NaCl solution confined in a nanochannel. Here we consider the walls with 8 units cells both in the x- and y-directions. (A unit cell is shown in Fig. 1(a).) Every four atoms in the direction of the shortest distance of the triangular lattice are negatively charged ($-e$).

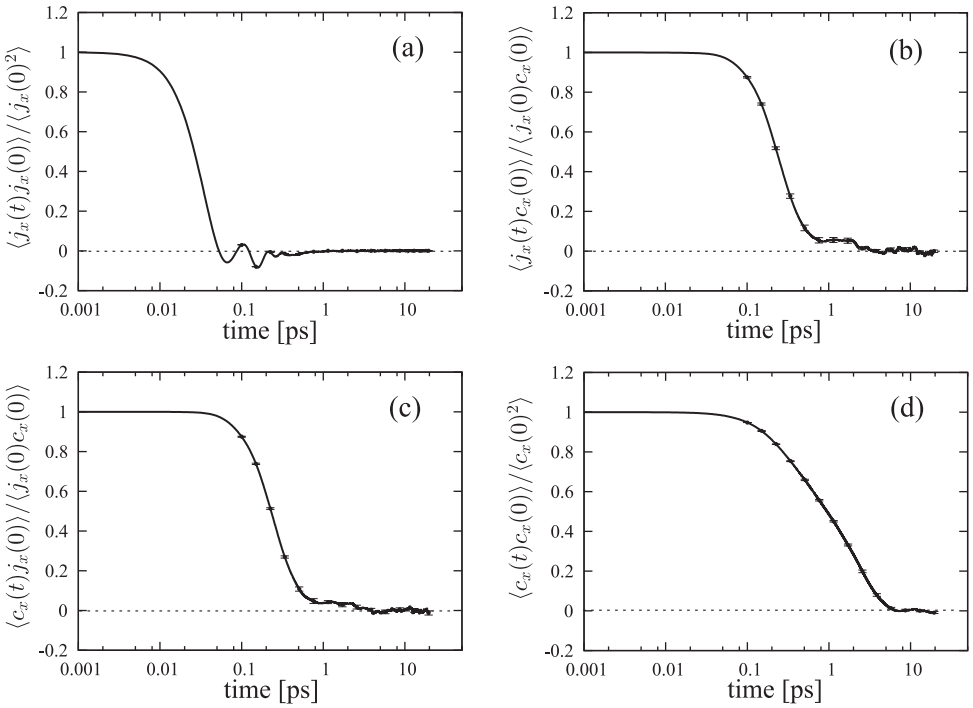

FIG. 2. Normalized time-correlation functions of the charge and mass fluxes: (a) charge-charge, (b) charge-mass, (c) mass-charge, and (d) mass-mass. Each curve is the average over ten simulation runs with different initial configurations, and the standard error is indicated with the error bar.

The surface charge density is then $\sigma = 0.128\,\mathrm{C/m^2}$. The gap between the walls contains 1260 water molecules with 24 Na^+ ions and 8 Cl^- ions. The charged wall atoms and the ions maintain the electrical neutrality. The distance between the upper and lower walls determined with the strategy described in Section II is $H = 41.1\,\text{Å}$, and the resulting molar concentrations of Na^+ and Cl^- are 0.97 M and 0.32 M, respectively.

In order to obtain the time-correlation functions of j_x and c_x necessary for Eqs. (11) through (14), the MD simulation at thermal equilibrium is performed for 5 ns, and the values of j_x and c_x are recorded every time step (1 fs). The correlations are taken for the time difference $0 \le t \le 20\,\mathrm{ps}$, and the 498×10^4 time-series samples are averaged. We have checked the influence of the initial configuration, and have observed considerable variations in the time-correlation functions, especially in $\langle j_x(t)j_x(0)\rangle$, $\langle j_x(t)c_x(0)\rangle$, and $\langle c_x(t)j_x(0)\rangle$. The variation due to the initial configuration was not suppressed even if we extended the simulation time to 20 ns and increased the number of the time-series samples. This is because the motion of ions in the electrolyte solution is slow (cf. Ref. 43), and very long simulation time is required to obtain the sufficient statistics in calculating the time-correlation functions

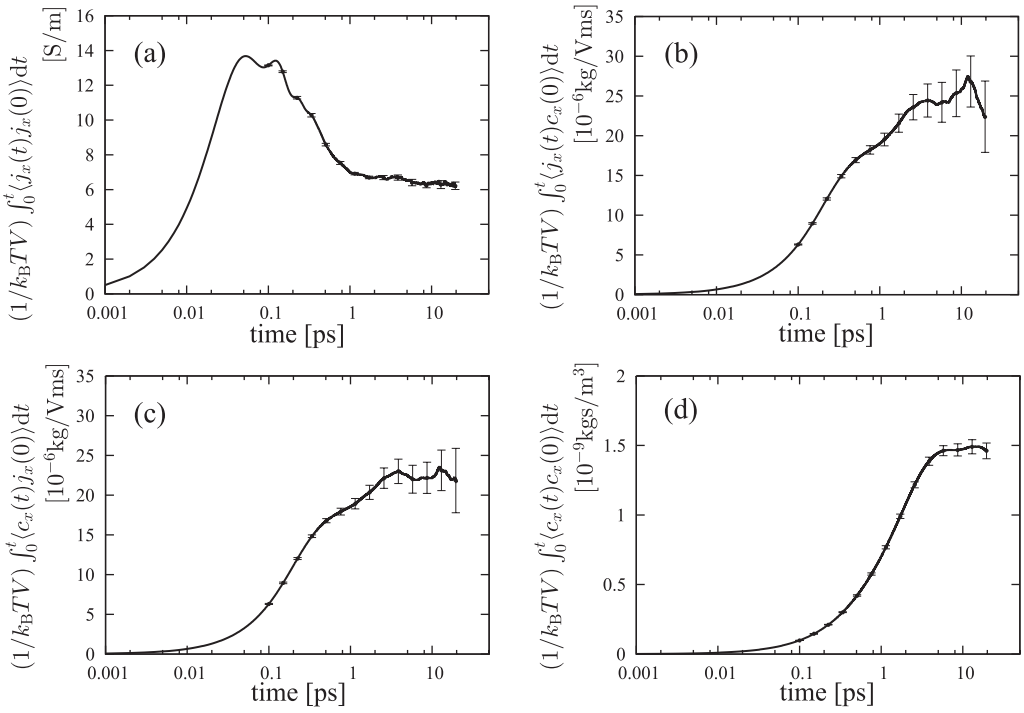

FIG. 3. Time-integrated correlation functions of the charge and mass fluxes: (a) charge-charge, (b) charge-mass, (c) mass-charge, and (d) mass-mass. The values are scaled by $k_{\mathrm{B}}TV$, so that their long-time limits directly correspond to the transport coefficients. See the caption of Fig. 2 for the meaning of the error bar.

in which the motion of the ions is important. In the present study, we circumvent this difficulty by carrying out ten MD simulations with different initial configurations, each of which runs for 5 ns. The ten time-averaged correlation functions are then averaged again, and the results are shown in Fig. 2. The error bar for ten simulation runs shows that the error due to a specific initial condition is greatly reduced. As shown in Fig. 3, however, if the correlation functions are integrated over very long time, the error accumulates and becomes significant. Therefore, the time-integration in Eq. (14) is terminated at 10 ps, and that in Eqs. (11) through (13) is terminated at 5 ps, in evaluating the transport coefficients listed in Table II. Onsager's reciprocal relation $M^{\mathrm{jm}} = M^{\mathrm{mj}}$ holds within the error of 6%, which gives a measure of reliability of the numerical evaluation.

We note here that for confined systems the definition of the system volume that is necessary in using Eqs. (11) through (14) is not unique. Here and in what follows, we use the volume computed from the distance between the upper and lower wall atoms. Another possibility could be to employ the domain actually occupied by the electrolyte solution as the

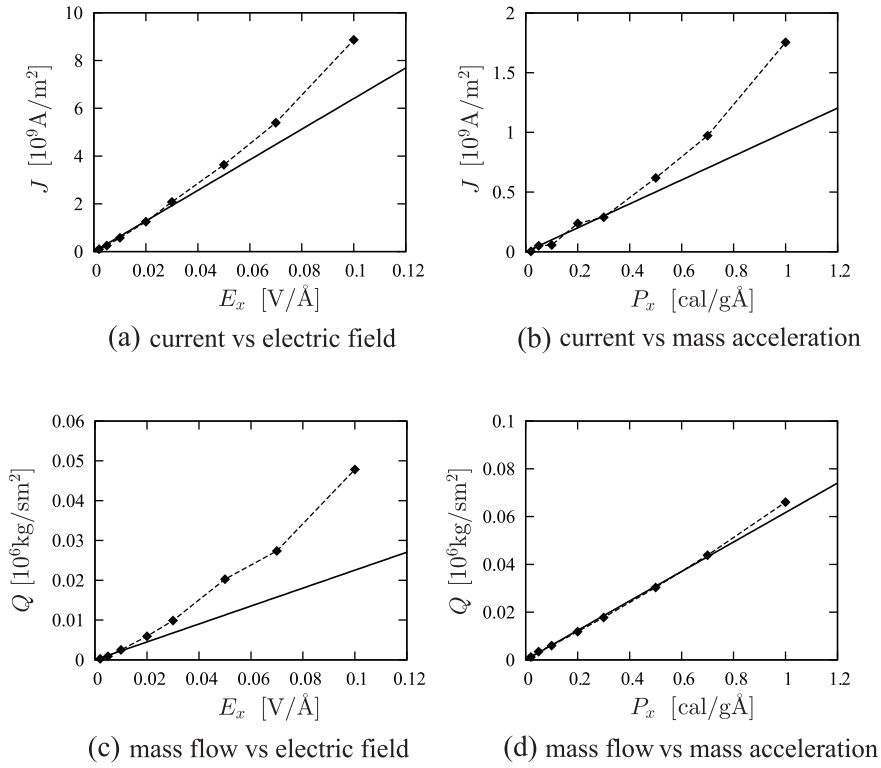

FIG. 4. Current and mass flow densities induced by the electric field or the mass acceleration. The symbol indicates the results of the simulations with the explicit external field, and the solid linear line indicates Eq. (1) with the transport coefficients obtained from the Green–Kubo formulas.

system volume. The latter is smaller because of the excluded volumes of the wall atoms, and using the latter yields difference in the transport coefficients by several percent. However, because the current density and mass flow density obtained from the direct method also include the system volume in the same manner ($J = j_x/V$ and $Q = c_x/V$), this difference does not affect the relative comparison of the two methods.

The current density J and mass flow density Q, which are computed using the transport coefficients in Table II via Eq. (1), are valid only within the linear response regime. In order to clarify quantitatively the range of the external field strength in which Eq. (1) is valid, we compare Eq. (1) with the values of J and Q obtained with the direct method. Figure 4 plots J and Q as functions of the external fields E_x and P_x. At each value of the external field strength, a 4 ns production run is carried out to average over the time-series data, after a simulation for 1 ns to reach the steady state. In the parameter range of Fig. 4, the fluxes in the direct method are obtained with better statistics than those in the simulations at thermal equilibrium, because the configuration of ions and water molecules is perturbed

TABLE II. Transport coefficients; values in parentheses are standard errors for ten simulation runs.

$M^{\rm jj}$ [S/m]	$M^{\rm jm}$ [10^{-6}kg/Vms]	$M^{\rm mj}$ [10^{-6}kg/Vms]	$M^{\rm mm}$ [10^{-9}kgs/m^3]
6.52 (0.15)	24.0 (2.38)	22.5 (1.7)	1.47 (0.05)

TABLE III. Parameters of the systems.

	system				
	1	2	3	4	5
σ [C/m^2]	0.057	0.082	0.128	0.228	0.514
$N_x \times N_y$	12×12	10×10	8×12	9×12	8×12
ℓ_c/ℓ	6	5	4	3	2
no. of charged wall atoms	16	16	24	48	96
no. of H_2O	2840	1980	1890	2130	1890
no. of Na^+	88	66	72	102	144
no. of Cl^-	72	50	48	54	48
H [Å]	42.3	42.4	41.9	41.2	40.7
$C_{\rm Na}$ [M]	1.54	1.66	1.91	2.44	3.93
$C_{\rm Cl}$ [M]	1.26	1.26	1.27	1.29	1.31
C_0 [M]	1.73	1.74	1.65	1.60	1.55

more significantly by the external fields. Therefore we used only one initial configuration to evaluate the fluxes at each value of the external field strength.

In Fig. 4, Eq. (1) with the values in Table II is also indicated by the solid line. Although the results of the direct method are generally larger than those obtained from Eq. (1), they approach asymptotically as $E_x \to 0$ and $P_x \to 0$. Particularly, the two results agree well in the range $E_x \le 0.02\,\mathrm{V/Å}$ and $P_x \le 0.2\,\mathrm{cal/gÅ}$. The minimum values of the external fields in the figure are $E_x = 0.002\,\mathrm{V/Å}$ and $P_x = 0.02\,\mathrm{cal/gÅ}$, which are extremely large values compared with the field strength attainable in laboratories. In MD simulations, very large external fields are usually necessary to distinguish the observed variables from the thermal fluctuations as in this case. Figure 4 confirms that even if the external field is unrealistically large, there exists the range in which the results of the direct method agree well with the results based on the linear response theory. On the other hand, it implies that extrapolating a result of one single computation of the direct method can cause serious errors when the external field is too strong, as in the range $E_x > 0.02\,\mathrm{V/Å}$ of Figs. 4(a) and (c), and in the range $P_x > 0.3\,\mathrm{cal/gÅ}$ of Fig. 4(b).

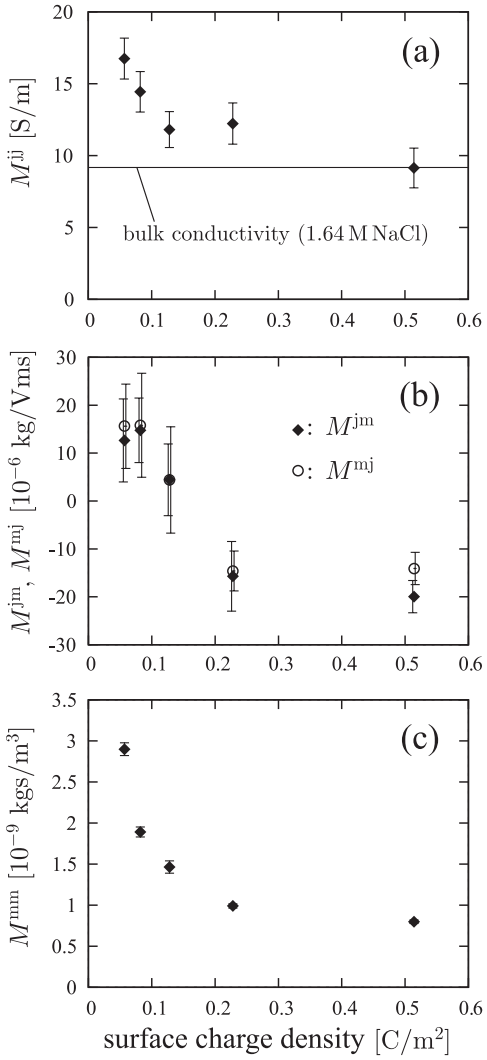

FIG. 5. Transport coefficients vs surface charge density for the systems listed in Table III. The error bar indicates the standard error for ten simulation runs. In panel (b), the error bars for $M^{\rm jm}$ and $M^{\rm mj}$ are slightly shifted to the left and right, respectively, for legibility.

B. Influence of the surface charge density

In this section, we consider five systems listed in Table III and investigate the influence of the surface charge density on the electrokinetic flows in nanochannels. Each wall consists of N_x and N_y unit cells (Fig. 1(a)) in the x- and y-directions, respectively, and a unit negative charge is assign to every ℓ_c/ℓ atoms in the direction of the shortest distance of the triangular lattice. The surface charge density of system 3 is identical to that of the system considered in the previous section, though the concentration of ions in the present section is higher. The number of water molecules contained between the gap is chosen such that the distance H is

within 41.5 ± 1 Å. The number of Cl^- ions is chosen for the ion concentration to be within 1.3 ± 0.05 M, and then the number of Na^+ is determined from the electrical neutrality, i.e., C_{Na} is increased as the surface charge density increases to compensate the negative surface charge, while C_{Cl} is kept at constant.

Since the concentration of ions is sufficiently high in the systems considered herein, the electrical double layers do not overlap, and there exists a region near the center of the channel where the profiles of concentration of Na^+ and Cl^- exhibit plateaus with a common value. The values of the concentration of the plateau region, denoted by C_0, are also listed in Table III.

The transport coefficients obtained with the protocol described in the previous subsection are plotted in Fig. 5. Here, the correlations for longer time interval ($0 \leq t \leq 100$ ps) than that in the previous subsection were taken in computing the transport coefficients. In order to interpret the results, the distribution of Na^+ is investigated. We show in Fig. 6 the radial distribution function $g(r)$ of Na^+ about the charged wall atom, along with the coordination number defined as $c_g(r) = 2\pi n_0 \int_0^r \tilde{r}^2 g(\tilde{r}) \mathrm{d}\tilde{r}$ with n_0 being the average number density of Na^+. Since the distribution of Na^+ is restricted to a half side of the wall atoms, the ions in a hemispherical shell is counted in obtaining $g(r)$. In addition to the radial distribution of Na^+, the distributions of Na^+ and Cl^- across the channel are also investigated. For this purpose, the local concentrations of ions, $C_{Na}(z)$ and $C_{Cl}(z)$, are evaluated by counting the ions within $z \pm 0.1$ Å during the simulation for 5 ns. Using the local concentration, the charge density distribution $\rho_e(z)$ and the PMFs $\psi_\alpha(z)$ (α =Na, Cl) are calculated through the following formulas[44] and plotted in Fig. 7:

$$\rho_e(z) = F(C_{Na}(z) - C_{Cl}(z)), \tag{15}$$

$$\psi_\alpha(z) = -k_B T \ln(C_\alpha(z)/C_0), \tag{16}$$

where F is the Faraday constant.

For comparison with the effective electrical conductivity M^{jj} shown in Fig. 5(a), the electrical conductivity of the bulk NaCl solution at concentration 1.64 M is computed from Eq. (11) with $\langle j_x(t) j_x(0) \rangle$ obtained from a simulation with periodic boundary conditions in the three directions. The electrical conductivity in the nanochannels is generally higher than the bulk conductivity, because of the surface conductivity. The excess conductivity

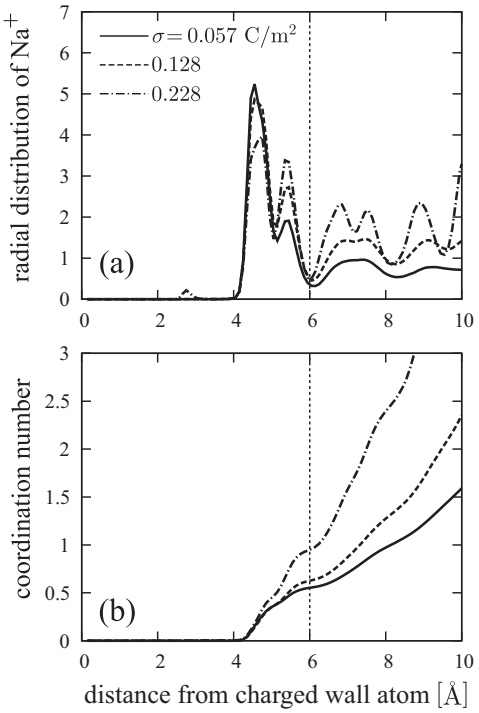

FIG. 6. (a) Radial distribution function (RDF) $g(r)$ of Na^+ about the charged wall atom. (b) Coordination number (or integrated RDF) $c_g(r)$.

is reduced as the surface charge density increases, in spite of the fact that the number of excess counter-ions increases. This is because the counter-ions are strongly bound due to the counter-ion condensation near the surface, and thus the contribution to the conductivity decreases. The behavior of the bound counter-ions is shown in Fig. 6: the radial distribution exhibits clear separation at $r = 6\,\text{Å}$, implying that the counter-ions within $r < 6\,\text{Å}$ are bound to a charged wall atom. The coordination number at $r = 6\,\text{Å}$ is the number of bound counter-ions per charged wall atom. It increases as the surface charge density increases, indicating a reduced number of free counter-ions for the high surface charge density.

The transport coefficients for the streaming current M^{jm} and the electro-osmotic flow M^{mj} are identical within the error, as shown in Fig. 5(b), which again confirms Onsager's reciprocal relation. Note that they are negative at $\sigma = 0.228$ and $0.514\,\text{C/m}^2$, i.e., the direction of the streaming current and the electro-osmotic flow are reversed. This is consistent with the reversal of the electro-osmotic flow reported in Ref. 27. The cause of the inversion is understood as follows: in the case of the large surface charge density, the counter-ions are strongly bound at the well of PMF at $z = 4.5\,\text{Å}$ (Fig. 7(b)), and the co-ions (Cl^-) are

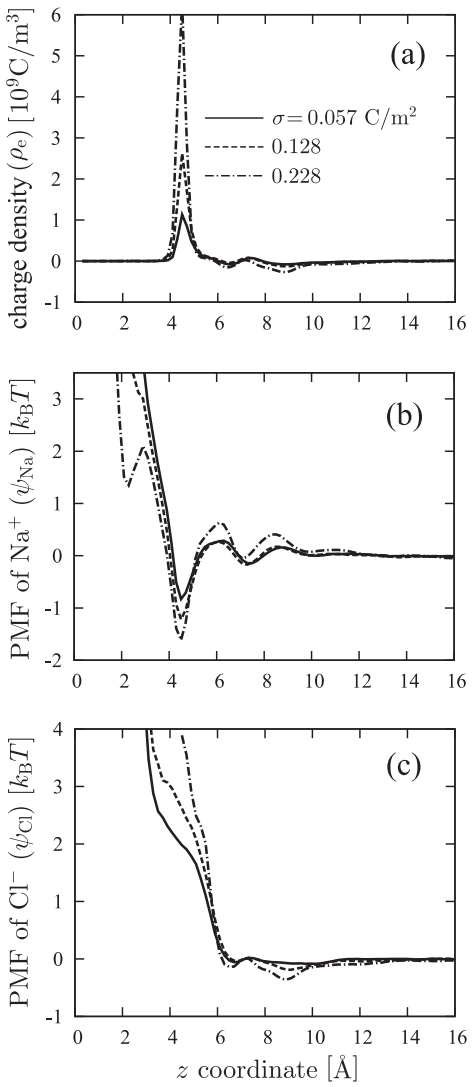

FIG. 7. Profiles in the z-direction of (a) the charge density, (b) the potential of mean force (PMF) for Na^+, and (c) that for Cl^-. The origin of the coordinate is at the position of the wall atoms.

then pushed toward the middle of the channel. The co-ions gather near the well of PMF at $z = 9\,\text{Å}$ shown in Fig. 7(c), to form the negatively charged region observed in Fig. 7(a). Responses of this negatively charged region to the mass acceleration and electric field result in the reversed streaming current and electro-osmotic flow.

We note here the contribution of the electro-osmotic flow to the surface conductivity observed in Fig. 5(a). In the case of the forward flow, the number of counter-ions in the mobile region is larger than that of co-ions, and the electric current in the forward direction is enhanced by the electro-osmosis. On the other hand, when the electro-osmotic flow is reversed, the number of co-ions exceeds that of counter-ions in the mobile region, increasing

the speed of negative charge in the reverse direction. The latter also contributes to the current in the forward direction, or the conductivity gain. Therefore, the main reason for the decreasing conductivity with increasing surface charge density observed in Fig. 5(a) is most probably the loss of mobile counter-ions due to the strong binding, as explained before.

Figure 5(c) shows that the rate of the Poiseuille-type flow induced by the mass acceleration decreases as the surface charge density increases. In order to investigate this flow reduction in greater details, in Fig. 8(a), we show the velocity profiles obtained with the direct method at $P_x = 0.2\,\mathrm{cal/g\AA}$. The electro-osmotic flows at $E_x = 0.02\,\mathrm{V/\AA}$ are also shown in Fig. 8(b). The values of the field strength are within the limit of the linear response regime (Fig. 4). The velocity at z is the mean velocity of all the atoms existing in the range $z \pm 0.5\,\mathrm{\AA}$, during the 4 ns simulation. For comparison, the velocity profiles of the continuum theory based on the Stokes equation and the Poisson–Boltzmann equation are also shown:[45]

$$u_x(z) = \frac{P_x \rho_0}{2\mu}\left(zH - z^2\right) + \frac{E_x \sigma}{\mu\kappa}\left(\frac{\cosh(\kappa H/2) - \cosh(\kappa(z - H/2))}{\sinh(\kappa H/2)}\right), \tag{17}$$

$$\kappa = \left(\frac{2C_0 eF}{\varepsilon_0 \varepsilon_r k_\mathrm{B} T}\right)^{1/2}, \tag{18}$$

where ε_0 is the permittivity of vacuum, and μ and ε_r are the viscosity and the dimensionless dielectric constant, respectively, of the electrolyte solution. For simplicity, we have assumed the stick boundary condition at the interface, and the uniform viscosity ($\mu = 0.72 \times 10^{-3}\,\mathrm{Pa\,s}$) and dielectric constant ($\varepsilon_r = 76.7$) of the SPC/E water molecules, which are listed in Table II of Ref. 46. An attempt to improve the continuum model using the non-uniform viscosity and dielectric constant with slip boundary condition is found in Ref. 47. Clearly, from Fig. 8(a), the molecules near the surfaces are immobile in the cases of large surface charge density. The previous results of the immobilization of the water molecules[38] and that of the counter-ion,[48] for large surface charge densities, are consistent with the present observation. Particularly, for $\sigma \geq 0.228\,\mathrm{C/m^2}$, the flow velocity is almost zero in $z \leq 5\,\mathrm{\AA}$. The effective narrow gap due to the immobilization of the molecules results in a decrease of the transport coefficients, as shown in Fig. 5(c).

The velocity profiles of the electro-osmotic flow are shown in Fig. 8(b), along with the continuum model at $\sigma = 0.057\,\mathrm{C/m^2}$. Obviously, in Eq. (17), the flow velocity of the

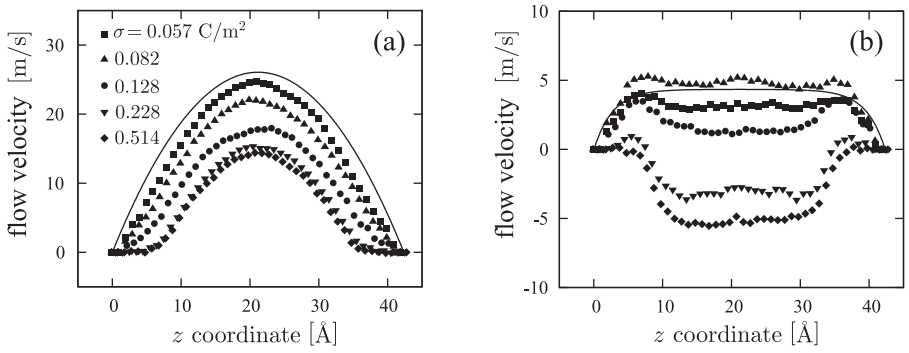

FIG. 8. Velocity profiles across the channel of (a) the Poiseuille-type flow at $P_x = 0.2\,\mathrm{cal/gÅ}$ and (b) the electro-osmotic flow at $E_x = 0.02\,\mathrm{V/Å}$. The solid line indicates the profiles predicted by the continuum theory (Eq. (17)); $\sigma = 0.057\,\mathrm{C/m^2}$ in panel (b).

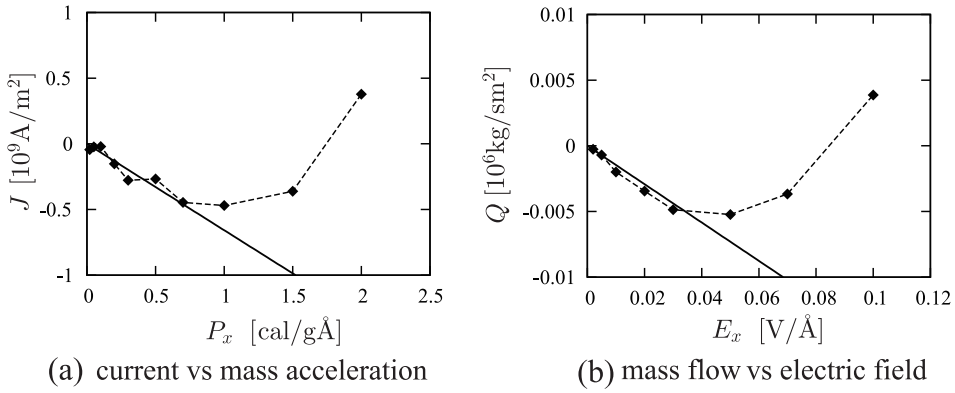

FIG. 9. (a) The current density induced by the mass acceleration, and (b) the mass flow density induced by the electric field, in the case of $\sigma = 0.228\,\mathrm{C/m^2}$. See the caption of Fig. 4.

continuum model increases in proportion to the surface charge density. On the contrary, the flow velocity obtained with the MD simulations decreases as the surface charge density increases, and the reversal of the flow takes place for $\sigma \geq 0.228\,\mathrm{C/m^2}$. This behavior of the electro-osmotic flow is perfectly consistent with the transport coefficients shown in Fig. 5(b). Although the driving force in the forward direction acts on the positively charged region $z \leq 5\,\mathrm{Å}$ (Fig. 7(a)), the molecules in this region do not move because of the strongly bound counter-ions for $\sigma \geq 0.228\,\mathrm{C/m^2}$, as in Fig. 8(b). Therefore, the force acting on the negatively charged region at $z = 9\,\mathrm{Å}$ (Fig. 7(a)) drives the flow in the opposite direction.

The observation above implies that the counter-ion condensation takes place for $\sigma \geq 0.228\,\mathrm{C/m^2}$, in view of the fact that the mobility of the counter-ions condensed at the

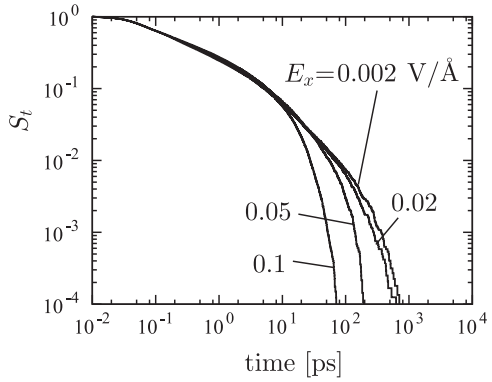

FIG. 10. Bond survival probability distribution S_t for a bond between an Na^+ ion and a negatively charged wall atom in the presence of the external electric field. The surface charge density is $\sigma = 0.228\,\mathrm{C/m^2}$.

interface is significantly lower than that of the weakly bound counter-ions.[49] The recent counter-ion condensation theory for plane surfaces by Manning predicts the critical value above which the counter-ions condense at the interface:[50]

$$\sigma_{\mathrm{crit}} = \frac{2\varepsilon_0\varepsilon_r k_{\mathrm{B}} T\kappa(-\ln\kappa l_{\mathrm{ref}})}{e^2}, \tag{19}$$

where l_{ref} is the characteristic length assumed to be small compared with the thickness of the electrical double layer; the possibility of identifying l_{ref} with the length scale of the molecular structure at the surface is discussed in Ref. 50. If we apply Eq. (19) to our case with assuming $l_{\mathrm{ref}} = 1$ Å, then the predicted critical value is $\sigma_{\mathrm{crit}} = 0.135\,\mathrm{C/m^2}$. Although the theory in Ref. 50 treats perfectly plane surface and states no dynamical property in the direction parallel to the surfaces, the consistency with the present simulation results ($\sigma_{\mathrm{crit}} = 0.128 \sim 0.228\,\mathrm{C/m^2}$), in conjunction with the previous results of the mobility of the condensed counter-ions in another geometry,[49] could shed light on the interplay between the counter-ion condensation and dynamical properties of the counter-ions adjacent to realistic plane surfaces.

We now examine the influence of the external field strength on the streaming current and electro-osmotic flow, which are reversed in the linear response regime. In Fig. 9, we plot J as a function of P_x, and Q as a function of E_x, for the case of $\sigma = 0.228\,\mathrm{C/m^2}$. Similarly to Fig. 4, J and Q asymptotically approach the results of the linear response theory as $E_x \to 0$ and $P_x \to 0$. They start to depart at $P_x = 1\,\mathrm{cal/g\AA}$ and $E_x = 0.05\,\mathrm{V/Å}$, and

TABLE IV. Parameters of the systems.

	system			
	$1'$	$2'$	$3'$	$4'$
σ [C/m^2]	0.057	0.082	0.128	0.228
no. of H_2O	2840	1980	1890	2130
no. of Na^+	74	52	49	54
no. of Cl^-	58	36	25	6
H [Å]	42.1	42.1	41.4	40.1
$C_{\rm Na}$ [M]	1.29	1.31	1.30	1.29
$C_{\rm Cl}$ [M]	1.01	0.90	0.66	0.14
C_0 [M]	1.55	1.17	1.08	0.15

the current and the mass flow change the direction at $P_x = 2\,\mathrm{cal/g\AA}$ and $E_x = 0.1\,\mathrm{V/\AA}$, respectively, because the bound counter-ions are pulled away from the surface charges by the strong external fields. The motion of the bound counter-ions is described in a quantitative manner using the bond survival probability distribution: $S_t(t) = 1 - \int_0^t P_t(s)\mathrm{d}s$ with $P_t(s)\mathrm{d}s$ being the probability that a counter-ion stays within 6 Å form a charged wall atom for time period s. Recall that the counter-ions within 6 Å are bound (see Fig. 6). The bond survival probability distribution is shown in Fig. 10 for some values of the external electric field at $\sigma = 0.228\,\mathrm{C/m^2}$. Clearly, the strong external electric field shortens the bond survival time, meaning that the counter-ions are dragged by the field.

Figure 9 clearly demonstrates that the property of the flows for the same system can drastically differ depending on the external field strength, implying that we should be careful in extrapolating the results of the direct method to realistic systems.

We conclude with a brief discussion on the concentration of the solution in the charged nanochannel. In the simulations for the systems listed in Table III, the counter-ions (Na^+ ions) were added to compensate the increasing surface charge density. We here explore the other possibility of compensating the increasing negative charge on the surface, namely, decreasing the concentration of the co-ions (Cl^- ions) while maintaining the concentration of the counter-ions (Na^+ ions) at constant. Table IV lists the simulation parameters used here. The configurations of the wall atoms in systems $1' \sim 4'$ are exactly the same as those of systems $1 \sim 4$ in Table III, respectively. The number of Na^+ ions is chosen such that the concentration falls within $1.3 \pm 0.05\,\mathrm{M}$, and then the number of Cl^- is determined from the charge neutrality.

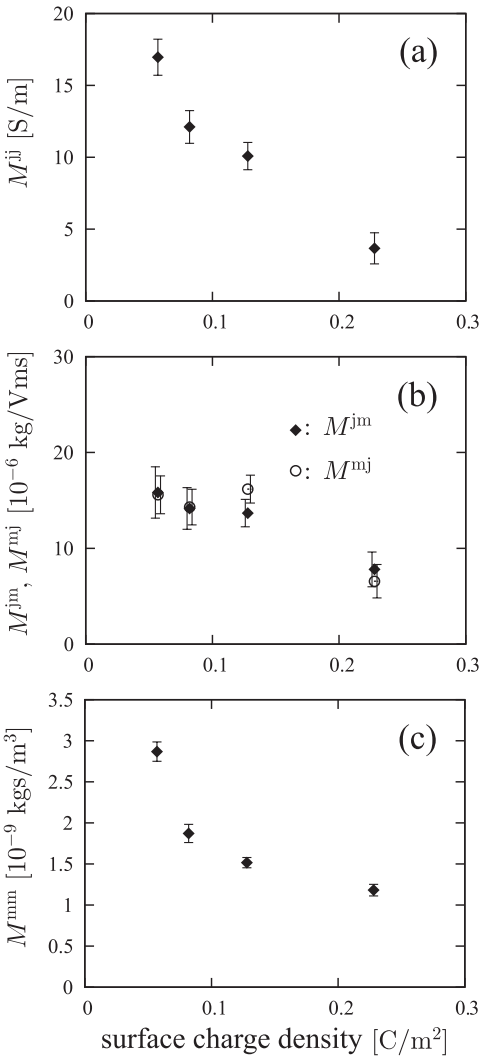

FIG. 11. Transport coefficients vs surface charge density for the systems listed in Table IV. See the caption of Fig. 5.

The transport coefficients of systems $1' \sim 4'$ are shown in Fig. 11. One obvious qualitative difference from Fig. 5 is the significant decrease of the conductivity at $\sigma = 0.228\,\mathrm{C/m^2}$ in Fig. 11(a). This decrease is caused by the fact that most of the counter-ions are condensed at the interface in the case of the high surface charge density, and the number of the mobile ions are greatly reduced. Indeed, the value of C_0, which represents the concentration in the mobile region, of system $4'$ is very small compared with that of system 4. Another important difference is that the reversal of the streaming current and the electro-osmotic flow does not occur at $\sigma = 0.228\,\mathrm{C/m^2}$ (Fig. 11(b)), i.e., $M^{\rm jm}$ and $M^{\rm mj}$ do not change their sign, although the values are slightly smaller than those for $\sigma < 0.228\,\mathrm{C/m^2}$. This is because the number

of co-ions is not sufficient to form the negatively charged region observed in Fig. 7(a).

If an experiment corresponding to the systems considered in the present study is performed for a setup with two reservoirs of constant concentration C_s connected by a nanochannel, C_0 will be comparable to C_s. Therefore, the systems listed in Table III are relevant because the value of C_0 is controlled such that it ranges within $1.65 \pm 0.1\,\mathrm{M}$, whereas the value of C_0 varies significantly in Table IV. It is then important to notice that the value of C_0 that is common to Na^+ and Cl^- is defined only if the thickness of the electrical double layer is sufficiently short compared with the channel width, as in the systems considered in the present paper; otherwise the concentration of Na^+ differs from that of Cl^- over the channel. In the latter case the Donnan effect manifests itself[51] and the concentration of Cl^- should decrease upon increasing the surface charge density (see, e.g., Ref. 13). Therefore care must be taken in setting the value of concentration for systems with different surface charge densities, depending on the circumstances, because the manner of changing the concentration has significant influence on the qualitative behavior of the electrolyte solution, as demonstrated by comparing Figs. 5 and 11.

V. SUMMARY

In the present paper, we have studied the currents and mass flows of an aqueous NaCl solution in nanochannels of the gap $\sim 40\,\text{Å}$ induced by an electric field and a mass acceleration corresponding to a pressure gradient. In order to accurately calculate the four transport coefficients through the Green–Kubo formulas, ten MD simulation runs with different initial configurations for each system are carried out to obtain smooth time-correlation functions. Comparison of the current and mass flow predicted by Eq. (1) with those obtained by the direct method revealed that, although extremely strong external fields led to large discrepancies, the two results converged within a range of external field strengths for which the flows were still distinguishable from the thermal fluctuation. In the present study, we considered the time-independent external fields. However, the responses to the time-dependent fields, such as oscillatory fields, can be also examined by means of both the Green-Kubo formulas and the direct method, the results of which should coincide in the linear response regime.[52]

One of the advantages of the direct method using nonequilibrium simulation is that the flow induced in the channel is obtained with better statistics than those in the simulation at

thermal equilibrium, because of significant perturbation due to the external fields. Therefore, generally the computational cost required to obtain the flow at a specified field strength is much less than that required to perform the time-integration in the Green–Kubo formulas, as discussed in Section IV A. However, extrapolating only a few results of the direct method can mislead us, as demonstrated in Fig. 9. A careful examination is inevitable to ascertain if the field strength is in the linear or non-linear regime, the cost of which can comparable with that for the Green–Kubo approach. Therefore, in studies on responses to external fields, it is preferable to first investigate the system properties through the Green–Kubo approach, followed by the additional computations to observe the flow directly, as has been done in Fig. 8, or to investigate the non-linear regime as necessary. A relevant discussion is found in a recent note on the computation of the bulk viscosity in Ref. 53.

The influence of the surface charge density of the channel walls was also examined, with maintaining the channel width and the concentration of Cl^- at constant. As a result, the effective electric conductivity and the rate of the Poiseuille-type flow were found to be reduced by the large surface charge density, because the excess Na^+ ions strongly bound near the interface interfered with the charge and mass flows. The reversal of the streaming current and the electro-osmotic flow was observed both in the transport coefficients obtained with the Green–Kubo formulas and in the results of the direct method, which is consistent with the finding reported in Ref. 27.

As an extension of the present study, it would be interesting to investigate the influence of the variety of the surfaces, for example, hydrophobic surfaces and more complicated chemically modified surfaces. Another direction of future studies could be to replace the solute and solvent by the more complex ones used in lithium ion batteries and fuel cells for understanding the nano-scale transport properties important in the state-of-the-art electrochemical devices. Our study shows that, apart from the computational cost in dealing with more complex systems (for which nonlinear effects may be even more important than shown here) and the difficulty in identifying the appropriate force fields, there is no principle difficulty in obtaining accurate values of the electro-osmotic coefficients at this scale using molecular dynamics.

ACKNOWLEDGMENTS

The authors are grateful to S. Iwai for computer assistance in preparing the manuscript. H. Y., T. K., and H. W. are supported by MEXT program "Elements Strategy Initiative to Form Core Research Center" (since 2012). (MEXT stands for Ministry of Education, Culture, Sports, Science, and Technology, Japan.) H. M. acknowledges support by the Nanosciences Foundation of Grenoble. J.-L. B. is supported by the Institut Universitaire de France, and acknowledges useful discussions with L. Bocquet and E. Charlaix.

REFERENCES

[1]B. Scrosati and J. Garche, "Lithium batteries: Status, prospects and future," J. Power Sources **195**, 2419–2430 (2010).

[2]S. J. Peighambardoust, S. Rowshanzamir, and M. Amjadi, "Review of the proton exchange membranes for fuel cell applications," Int. J. Hydrogen Energy **35**, 9349–9384 (2010).

[3]E. Kjeang, N. Djilali, and D. Sinton, "Microfluidic fuel cells: A review," J. Power Sources **186**, 353–369 (2009).

[4]A. Siria, P. Poncharal, A.-L. Biance, R. Fulcrand, X. Blase, S. T. Purcell, and L. Bocquet, "Giant osmotic energy conversion measured in a single transmembrane boron nitride nanotube," Nature **494**, 455–458 (2013).

[5]N. Baba, H. Yoshida, M. Nagaoka, C. Okuda, and S. Kawauchi, "Numerical simulation of thermal behavior of lithium-ion secondary batteries using the enhanced single particle model," J. Power Sources **252**, 214–228 (2014).

[6]J. Newman, *Electrochemical Systems*, 2nd ed. (Prentice-Hall, Englewood Cliffs, NJ, 1991).

[7]E. Brunet and A. Ajdari, "Generalized onsager relations for electrokinetic effects in anisotropic and heterogeneous geometries," Phys. Rev. E **69**, 016306 (2004).

[8]The flux of one ion component (cation or anion) is another important response of the present system, and then the corresponding external field is the chemical potential gradient of that component; although in the present paper we restrict ourselves to investigating two fluxes, i.e., the current and mass flow, to cover the transport coefficients of 3×3 matrix is a possible extension of this work.

[9]J. Bear, *Dynamics of fluids in porous media* (Dover Publications, 1988).

[10]L. Onsager, "Reciprocal relations in irreversible processes. 1." Phys. Rev. **37**, 405–426 (1931); "Reciprocal relations in irreversible processes. 2." **38**, 2265–2279 (1931).

[11]S. R. De Groot and P. Mazur, *Non-equilibrium Thermodynamics* (North-Holland, Amsterdam, 1962) ; republished by Dover, New York, 1984.

[12]J.-P. Hansen and I. R. McDonald, *Theory of Simple Liquids*, 3rd ed. (Academic Press, 2006).

[13]L. Bocquet and E. Charlaix, "Nanofluidics, from bulk to interfaces," Chem. Soc. Rev. **39**, 1073–1095 (2010).

[14]J. R. Looker and S. L. Carnie, "Homogenization of the ionic transport equations in periodic porous media," Transp. Porous Media **65**, 107–131 (2006).

[15]G. Allaire, R. Brizzi, J.-F. Dufrêche, A. Mikelić, and A. Piatnitski, "Ion transport in porous media: derivation of the macroscopic equations using upscaling and properties of the effective coefficients," Comput. Geosci. **17**, 479–495 (2013).

[16]A. Obliger, M. Duvail, M. Jardat, D. Coelho, S. Békri, and B. Rotenberg, "Numerical homogenization of electrokinetic equations in porous media using lattice-Boltzmann simulations," Phys. Rev. E **88**, 013019 (2013).

[17]G. Karniadakis, A. Beskok, and N. Aluru, *Microflows and Nanoflows* (Springer, 2005).

[18]Z. Zheng, D. J. Hansford, and A. T. Conlisk, "Effect of multivalent ions on electroosmotic flow in micro- and nanochannels," Electrophoresis **24**, 3006–3017 (2003).

[19]B. Rotenberg and I. Pagonabarraga, "Electrokinetics: insights from simulation on the microscopic scale," Mol. Phys. **111**, 827–842 (2013).

[20]L. Bocquet and J.-L. Barrat, "Hydrodynamic boundary conditions, correlation functions, and Kubo relations for confined fluids," Phys. Rev. E **49**, 3079–3092 (1994).

[21]V. Marry, J.-F. Dufrêche, M. Jardat, and P. Turq, "Equilibrium and electrokinetic phenomena in charged porous media from microscopic and mesoscopic models: electro-osmosis in montmorillonite," Mol. **101**, 3111–3119 (2003).

[22]L. Bocquet and J.-L. Barrat, "On the Green–Kubo relationship for the liquid-solid friction coefficient," J. Chem. Phys. **139**, 044704 (2013).

[23]I. F. Macdonald, M. S. El-Sayed, K. Mow, and F. A. L. Dullien, "Flow through porous media — the Ergun equation revisited," Ind. Eng. Chem. Fundamen. **18**, 199–208 (1979).

[24]R. Sadr, M. Yoda, Z. Zheng, and A. T. Conlisk, "An experimental study of electro-osmotic flow in rectangular microchannels," J. Fluid Mech. **506**, 357–367 (2004).

[25]D. J. Evans and G. Morriss, *Statistical mechanics of nonequilibrium liquids*, 2nd ed. (Cambridge University Press, 2008).

[26]S. Bernardi, S. J. Brookes, D. J. Searles, and D. J. Evans, "Response theory for confined systems," The Journal of chemical physics **137**, 074114 (2012).

[27]R. Qiao and N. R. Aluru, "Charge inversion and flow reversal in a nanochannel electroosmotic flow," Phys. Rev. Lett. **92**, 198301 (2004).

[28]D. M. Huang, C. Cottin-Bizonne, C. Ybert, and L. Bocquet, "Aqueous electrolytes near hydrophobic surfaces: Dynamic effects of ion specificity and hydrodynamic slip," Langmuir **24**, 1442–1450 (2008).

[29]D. M. Huang, C. Cottin-Bizonne, C. Ybert, and L. Bocquet, "Massive amplification of surface-induced transport at superhydrophobic surfaces," Phys. Rev. Lett. **101**, 064503 (2008).

[30]J. Liu, M. Wang, S. Chen, and M. O. Robbins, "Molecular simulations of electroosmotic flows in rough nanochannels," J. Comput. Phys. **229**, 7834–7847 (2010).

[31]A. Botan, V. Marry, B. Rotenberg, P. Turq, and B. Noetinger, "How electrostatics influences hydrodynamic boundary conditions: Poiseuille and electro-osmostic flows in clay nanopores." J. Phys. Chem. C **117**, 978–985 (2013), erratum: ibid, **117** 20376.

[32]H. Washizu and K. Kikuchi, "Electrical polarizability of polyelectrolytes in salt-free aqueous solution," J. Phys. Chem. B **106**, 11329–11342 (2002).

[33]G. S. Manning, "Counterion condensation theory of attraction between like charges in the absence of multivalent counterions," Eur. Phys. J. E **34**, 132 (2011).

[34]H. J. C. Berendsen, J. R. Grigera, and T. P. Straatsma, "The missing term in effective pair potentials," J. Phys. Chem. **91**, 6269–6271 (1987).

[35]D. E. Smith and L. X. Dang, "Computer simulations of NaCl association in polarizable water," J. Chem. Phys. **100**, 3757–3766 (1994).

[36]M. P. Allen and D. J. Tildesley, *Computer Simulation of Liquids* (Oxford Univ. Press, Oxford, 1989).

[37]A. Pertsin and M. Grunze, "A computer simulation study of stick-slip transitions in water films confined between model hydrophilic surfaces. 1. Monolayer films," Langmuir **24**, 135–141 (2008).

[38]B. Siboulet, J. Molina, B. Coasne, P. Turq, and J.-F. Dufrêche, "Water self-diffusion at the surface of silica glasses: effect of hydrophilic to hydrophobic transition," Mol. Phys.

111, 3410–3417 (2013).

[39]`http://lammps.sandia.gov`.

[40]S. Plimpton, "Fast parallel algorithms for short-range molecular dynamics," J. Comput. Phys. **117**, 1–19 (1995).

[41]J.-P. Ryckaert, G. Ciccotti, and H. J. C. Berendsen, "Numerical integration of the cartesian equations of motion of a system with constraints: molecular dynamics of n-alkanes," J. Comput. Phys. **23**, 327–341 (1977).

[42]I.-C. Yeh and M. L. Berkowitz, "Ewald summation for systems with slab geometry," J. Chem. Phys. **111**, 3155–3162 (1999).

[43]A. P. Lyubartsev and A. Laaksonen, "Concentration effects in aqueous NaCl solutions. a molecular dynamics simulation," J. Phys. Chem. **100**, 16410–16418 (1996).

[44]D. Chandler, *Introduction to Modern Statistical Mechanics* (Oxford University Press, 1987).

[45]H. Yoshida, T. Kinjo, and H. Washizu, "Coupled lattice Boltzmann method for simulating electrokinetic flows: a localized scheme for the Nernst–Plank model," Commun. Nonlinear Sci. Numer. Simulat. **in press** (2014), 10.1016/j.cnsns.2014.03.005.

[46]Y. Wu, H. L. Tepper, and G. A. Voth, "Flexible simple point-charge water model with improved liquid-state properties," J. Chem. Phys. **124**, 024503 (2006).

[47]D. J. Bonthuis and R. R. Netz, "Unraveling the combined effects of dielectric and viscosity profiles on surface capacitance, electro-osmotic mobility, and electric surface conductivity," Langmuir **28**, 16049–16059 (2012).

[48]R. R. Netz, "Electrofriction and dynamic Stern layers at planar charged surfaces," Phys. Rev. Lett. **91**, 138101 (2003).

[49]H. Washizu and K. Kikuchi, "Electric polarizability of DNA in aqueous salt solution," J. Phys. Chem. B **110**, 2855–2861 (2006).

[50]G. S. Manning, "The interaction between a charged wall and its counterions: a condensation theory," J. Phys. Chem. B **114**, 5435–5440 (2010).

[51]Note that according to Ref. 13 Donnan effects could appear as soon as the channel width becomes comparable to the Dukhin length σ/FC_0; in our case this length is indeed comparable to the width for the highest charge densities, which highlights the importance of considering the possibility of a reduction in free salt concentration.

[52]H. Mizuno and R. Yamamoto, "Mechanical responses and stress fluctuations of a super-

cooled liquid in a sheared non-equilibrium state," Eur. Phys. J. E **35**, 29 (2012).

[53]T. Chen, B. Smit, and A. T. Bell, "Are pressure fluctuation-based equilibrium methods really worse than nonequilibrium methods for calculating viscosities?" J. Chem. Phys. **131**, 246101 (2009).